5. Implementation of the CMS-EXO-19-002 analysis (physics beyond the Standard Model with multileptons; 137 fb^{-1})

By Eric Conte and Robin Ducrocq

5.1. *Introduction*

In this document, we present the implementation of the CMS-EXO-19-002 analysis [20] in the MadAnalysis 5 framework [3,6–8]. It consists of a search for events featuring multiple charged leptons, and relies on an integrated luminosity of 137 fb^{-1} of LHC proton-proton collisions, with a center-of-mass energy $\sqrt{s} = 13$ TeV.

In this analysis, two classes of models are targetted, which leads to the definition of two categories of signal regions. These consist of a type-III seesaw model [98] including three heavy fermions mediator $\Sigma^{\pm}$ and Σ^0, and a simple extension of the Standard model, called $t\bar{t}\phi$, with one scalar (or pseudoscalar) ϕ that can be produced in association with a top-antitop pair [99,100]. The type-III seesaw signal under consideration arises from the production and decay of $(\Sigma^{\pm}\Sigma^0)$ and $(\Sigma^{\pm}\Sigma^{\mp})$ pairs ($\Sigma^0\Sigma^0$ being neglected) in a multilepton final state. On the other hand, the $t\bar{t}\phi$ process with a $\phi \to l^+l^-$ decay induces a signal comprising additional b-jets originating from the top decays. The search for such signals is done in three ($3L$) and four ($4L$) leptons channels, with extra b-jets in the case of the $t\bar{t}\phi$ signal. For the validation of the implementation, we take into account predictions and official results with heavy fermion masses of $m_\Sigma = 300$ GeV and $m_\Sigma = 700$ GeV for the type-III seesaw benchmark, and masses of $m_\phi = 20$ GeV ($m_\phi = 70$ GeV) for the scalar (pseudoscalar) $t\bar{t}\phi$ model, as the CMS collaboration only provided material for those cases.

In section 5.2, we describe the selection and the manner in which the analysis is implemented in MadAnalysis 5. In particular, we present all signal regions defined in the CMS paper. Sections 5.3 and 5.4 are devoted to the validation of the implementation of the type-III seesaw and $t\bar{t}\phi$ signal regions respectively. We summarize our main results in section 5.5.

5.2. *Description of the analysis*

5.2.1. *Object definitions*

Muons are required to have a transverse momentum $p_T > 10$ GeV and a pseudorapidity $|\eta| < 2.4$. Requirements on the tracking quality are not implemented, as the package Delphes 3 that we use for the fast simulation of the CMS detector [9] is not able to reproduce it. To suppress the background, an isolation criterion is applied on the muons. The corresponding procedure relies on a relative isolation variable, Isol(l), defined as the scalar p_T sum of all particle-flow objects in a cone of $\Delta R = 0.4$ around the lepton direction and normalized to the lepton p_T. This variable,

$$\text{Isol}(l) = \frac{1}{p_T(l)} \sum_{j \neq l}^{\Delta R < 0.4} p_T(j) \quad \text{with } l \text{ being the lepton and } j \text{ any particle flow object,} \tag{5.1}$$

must be smaller than 15%. The displacement of the muon track with respect to the primary vertex is also constrained,

$$|d_z| < 0.1 \text{ cm} , \qquad |d_{xy}| < 0.05 \text{ cm}. \tag{5.2}$$

Electrons are required to have a $p_T > 10$ GeV, and a pseudorapidity $|\eta| < 2.5$ that is consistent with the tracking system acceptance. Requirements on the electron shower shape and track quality are not implemented. The relative isolation ratio as been chosen to be smaller than 15%, and is calculated with a cone of $\Delta R = 0.3$ around the electron. The displacement of the electron track with respect to the primary vertex is also constrained:

- $|d_z| < 0.1$ cm and $|d_{xy}| < 0.05$ cm when the electron is in the eletromagnetic calorimeter (ECAL) barrel acceptance ($|\eta| < 1.479$);
- $|d_z| < 0.2$ cm and $|d_{xy}| < 0.1$ cm when electron is in the ECAL barrel endcap ($|\eta| > 1.479$).

Finally, electrons that are too close to a muon (possibly due to bremsstrahlung from the muon) must be rejected. It is done by searching if there is a muon track in a cone around the electron track with a radius $\Delta R = 0.05$.

Jets are defined by using the anti-k_T algorithm [42] with a distance parameter of 0.4, as provided by the FastJet package [43,44]. They must have a $p_T > 30$ GeV and a $|\eta| < 2.1$. No pile-up simulation has been encapsulated because

we assume that pile-up suppression algorithms are good enough to get rid of all related soft contamination. Moreover, all jets which are inside a cone of radius $\Delta R = 0.4$ around a selected charged lepton are discarded.

We call '*b*-jets' the reconstructed jets originating from *B*-hadrons. The *b*-tagging performance in this CMS analysis corresponds to the medium working point of the DeepCSV algorithm [88], with an efficiency of 60–75% and a misidentification rate of 10% for *c*-quark jets and 1% for lighter jets.

In trilepton events, additional constraints are imposed on the charged leptons in order to reduce misidentified-background contributions. If a charged lepton can be matched which a loose *b*-jet (defined by a jet with p_T greater than 10 GeV, $|\eta| \leq 2.5$ and a medium *b*-tag), by using a matching cone of $\Delta R < 0.4$ around the lepton, the lepton is rejected. Besides, an additional selection cut based on a tri-dimensional impact parameter is also applied on the leptons. The lack of information relative to this quantity implies that we have not implemented this cut in the recast analysis.

Finally, the missing transverse momentum, noted MET or p_T^{miss}, is taken as the negative vector sum of all particle-flow objects p_T.

5.2.2. *Common event selection*

The trigger requirements imply an online selection of the events. This two-stage selection requires at least one electron or one muon in the event with a large p_T value. The first step of the offline selection consists of requiring one leading lepton with a threshold a little bit greater than the online selection threshold, and thus encapsulates the online selection. The p_T threshold value used in the offline selection depends on the year of data acquirement. For muons, the threshold is 26 GeV for 2016, 29 GeV for 2017 and goes back to 26 GeV for 2018. For electrons, the threshold is 30 GeV for 2016 and 35 GeV for 2017 and 2018. Considering the integrated luminosity recorded by CMS (37.80 fb^{-1} for 2016, 44.98 fb^{-1} for 2017 and 63.67 fb^{-1} for 2018), we apply a threshold of 26 GeV for 69% of the events (randomly chosen according to a flat distribution) and 29 GeV for the remaining events. Similarly, an electron threshold of 35 GeV is fixed for 74% of the events and 30 GeV for the remaining events.

We select events with three leptons (electrons or muons) or more. In the case where we have four leptons or more, we only keep the four leading leptons and label those events as "4 leptons" events.

All events containing a lepton pair where the two leptons are distant by $\Delta R < 0.4$ are rejected. We also remove events that contain a same-flavor lepton pair (independent of the charge) whose invariant mass is below 12 GeV. These two selection cuts allow us to remove low-mass resonances and final-state radiation background contributions.

In the case of a trilepton event, an additional constraint is applied. If the invariant mass of the three leptons is within the Z mass window (91 ± 15 GeV), the presence of an opposite-sign same-flavor (OSSF) lepton pair with an invariant mass below 76 GeV yields the rejection of the event. This procedure allows us to remove $Z \to l^+l^-\gamma$ background contributions where the photon converts into two additional leptons, with one of which being lost.

5.2.3. *Event selection and categorization devoted to the type-III seesaw signal*

The events are categorised in 7 signal regions according to:

- the number of selected leptons (three or four leptons) in the event,
- the number of opposite-sign same-flavor lepton pairs (OSSF multiplicity),
- the value of the invariant mass of the OSSF lepton pair relative to the Z mass window (91 ± 15 GeV). If there are several OSSF pairs, the considered invariant mass is the one which is the closest to the Z nominal mass. We refer the three cases as below-Z, on-Z and above-Z.

Table 5.1 collects the definition of the different signal regions.

Some signal regions involve an extra cut. The region called '*3L on-Z*' is populated by events that must feature a missing transverse energy MET greater than 100 GeV. Moreover, the region called '*4L OSSF2*' is populated by events containing either a missing transverse energy MET greater than 100 GeV, or no double OSSF lepton pairs on-Z.

Label	N_l	N_{OSSF}	M_{OSSF}	additional cut
3L below-Z	3	1	< 76 GeV	-
3L on-Z	3	1	$\in [76; 106]$ GeV	MET > 100 GeV
3L above-Z	3	1	> 106 GeV	-
3L OSSF0	3	0	-	-
4L OSSF0	≥ 4	0	-	-
4L OSSF1	≥ 4	1	-	-
4L OSSF2	≥ 4	2	-	MET > 100 GeV or no double OSSF on-Z

Table 5.1: List of the signal regions dedicated to probing the type-III seesaw model.

5.2.4. *Event selection and categorisation devoted to the $t\bar{t}\phi$ signal*

First, events that contain no opposite-sign same-flavor charged lepton pairs are rejected. Then, we denote the invariant mass of the OSSF pair M_{OSSF}. If there are several OSSF pairs, then we consider the invariant mass that is the closest to the Z nominal mass. Events that feature an M_{OSSF} in the Z mass window (91 ± 15 GeV) are rejected. Theses requirements make the signal regions orthogonal to all control regions defined in the considered CMS analysis.

Then, events are categorised into 18 signal regions according to:

- the number of selected leptons (three or four leptons),
- the number of opposite-sign same-flavor lepton pair (OSSF multiplicity),
- the flavor of the leptons involved in the computation of M_{OSSF},
- the b-jet multiplicity,
- the observable S_T defined as the scalar p_T sum of all jets, all charged leptons and the missing transverse momentum.

Table 5.2 collects the definition of the different signal regions.

5.3. *Validation of the implementation of the type-III seesaw signal regions*

5.3.1. *Event generation*

In the context of the type-III seesaw model, neutrinos are Majorana particles whose mass arises from interactions with new massive fermions organized in an $SU(2)$ triplet comprising heavy Dirac charged leptons ($\Sigma^{\pm}$) and a heavy Majorana neutral lepton (Σ^0).

The model has been already implemented in FeynRules [45] and is available in the form of a UFO [93,98] model. With MadGraph5_aMC@NLO [46], we consider the leading-order (LO) production of pairs of new fermions $\Sigma^{\pm}\Sigma^0$ and $\Sigma^+\Sigma^-$, $\Sigma^0\Sigma^0$ production being neglected. We assume two different values for the new physics masses of 300 GeV and 700 GeV, and we use the NNPDF3.0 LO [95] parton distribution functions (PDFs) provided by the LHAPDF package [50]. The cross section is rescaled at NLO+NLL and set to 0.5771 ± 0.0398 pb for the 300 GeV case and 0.01395 ± 0.00150 pb for the 700 GeV case [98,101].

Each new particle can then decay into a boson $V = h$, $W^{\pm}$ or Z, and a lepton of flavor l through a coupling denoted V_l. Following this scheme, a $\Sigma^{\pm}$ can decay into a $Z + l^{\pm}$, $h + l^{\pm}$ or $W^{\pm}\nu$ system, and a Σ^0 can decay into a $Z + \nu$, $h + \nu$ and a $W^{\pm}l^{\mp}$ system. The branching ratios are identical across all leptons flavors according to the *flavor-democratic scenario* obtained by taking the coupling V_e, V_μ and V_τ all equal to 10^{-4}. Their values have been computed and are given by Table 5.3. The tau channels are also considered through their leptonic decays. This decay has been implemented at the MadGraph5_MC@NLO level, but all boson decays are handled by Pythia 8 [51].

Pythia 8 also handles parton showering, hadronization, and the underlying events (multiple interaction and beam remnant interactions). We choose the CUETP8M1 tune [102] and the simulation of the detector response is handled by Delphes 3 [9], as driven through the MadAnalysis 5 platform.

The list of produced samples and the number of generated events for our validation procedure are given in Table 5.4.

Label	OSSF flavor	N_l	N_b	S_T
3L(ee) 0B ST<400	e	3	0	<400 GeV
3L($\mu\mu$) 0B ST<400	μ	3	0	<400 GeV
3L(ee) 0B 400<ST<800	e	3	0	∈[400;800] GeV
3L($\mu\mu$) 0B 400<ST<800	μ	3	0	∈[400;800] GeV
3L(ee) 0B ST>800	e	3	0	>800 GeV
3L($\mu\mu$) 0B ST>800	μ	3	1	<400 GeV
3L(ee) 1B ST<400	e	3	1	<400 GeV
3L($\mu\mu$) 1B ST<400	μ	3	1	<400 GeV
3L(ee) 1B 400<ST<800	e	3	1	∈[400;800] GeV
3L($\mu\mu$) 1B 400<ST<800	μ	3	1	∈[400;800] GeV
3L(ee) 1B ST>800	e	3	1	>800 GeV
3L($\mu\mu$) 1B ST>800	μ	3	1	>800 GeV
4L(ee) 0B ST<400	e	≥ 4	0	<400
4L($\mu\mu$) 0B ST<400	μ	≥ 4	0	<400
4L(ee) 0B ST>400	e	≥ 4	0	>400
4L($\mu\mu$) 0B ST>400	μ	≥ 4	0	>400
4L(ee) 1B	e	≥ 4	1	-
4L($\mu\mu$) 1B	μ	≥ 4	1	-

Table 5.2: List of the signal regions dedicated to probing the $t\bar{t}\phi$ model.

Process	Decay width formula	BR $m_\Sigma = 300$ GeV	BR $m_\Sigma = 700$ GeV
$\Gamma\left(\Sigma^0 \to l^\pm W^\pm\right)$	$\frac{g^2}{32\pi}\lvert V_l\rvert^2 \frac{M_\Sigma^3}{M_W^2}\left(1-\frac{M_W^2}{M_\Sigma^2}\right)^2\left(1+2\frac{M_W^2}{M_\Sigma^2}\right)$	71.6 %	66.2%
$\Gamma\left(\Sigma^0 \to \nu_l Z\right)$	$\frac{g^2}{64\pi c_W^2}\lvert V_l\rvert^2 \frac{M_\Sigma^3}{M_Z^2}\left(1-\frac{M_Z^2}{M_\Sigma^2}\right)^2\left(1+2\frac{M_Z^2}{M_\Sigma^2}\right)$	3.6%	2.8%
$\Gamma\left(\Sigma^0 \to \nu_l H\right)$	$\frac{g^2}{64\pi}\lvert V_l\rvert^2 \frac{M_\Sigma^3}{M_W^2}\left(1-\frac{M_H^2}{M_\Sigma^2}\right)^2$	24.8%	31.0%
$\Gamma\left(\Sigma^\pm \to \nu_l W^\pm\right)$	$\frac{g^2}{32\pi}\lvert V_l\rvert^2 \frac{M_\Sigma^3}{M_W^2}\left(1-\frac{M_W^2}{M_\Sigma^2}\right)^2\left(1+2\frac{M_W^2}{M_\Sigma^2}\right)$	35.0%	31.1%
$\Gamma\left(\Sigma^\pm \to l^\pm Z\right)$	$\frac{g^2}{64\pi c_W^2}\lvert V_l\rvert^2 \frac{M_\Sigma^3}{M_Z^2}\left(1-\frac{M_Z^2}{M_\Sigma^2}\right)^2\left(1+2\frac{M_Z^2}{M_\Sigma^2}\right)$	52.9%	54.3%
$\Gamma\left(\Sigma^\pm \to l^\pm H\right)$	$\frac{g^2}{64\pi}\lvert V_l\rvert^2 \frac{M_\Sigma^3}{M_W^2}\left(1-\frac{M_H^2}{M_\Sigma^2}\right)^2$	12.1%	14.6%

Table 5.3: Width expression [98] and branching ratio values relative to the new massive fermions Σ decay into a boson and a lepton (in the case where all V_l are equal)

5.3.2. *Comparison with the official CMS results*

The CMS paper does contain any cutflow-chart for the validation of the recast. This is the reason why the validation will be performed below on the principle of comparison of distributions of key observables at the end of the selection. All data used to build these plots is available from the HepData service [101, 103] and is used for the validation of the recast analysis. In other words, we will compare the distributions obtained at the end of the selection with the ones presented in Figures 3 and 4 of the CMS analysis note. For 6 out of 7 signal regions, we consider the distribution

Σ mass	lepton flavor	Number of produced events
300 GeV	$\mu\mu$	1,000,000
	ee	1,000,000
	$\tau\tau$	1,000,000
	$e\mu$	1,000,000
	$\tau\mu$	1,000,000
	τe	1,000,000
700 GeV	$\mu\mu$	1,000,000
	ee	1,000,000
	$\tau\tau$	1,000,000
	$e\mu$	1,000,000
	$\tau\mu$	1,000,000
	τe	1,000,000

Table 5.4: List of produced signal samples for the validation of the type-III seesaw signal regions.

of the quantity $L_T + p_T^{miss}$, where L_T is defined as the scalar sum of the p_T of all selected charged leptons and the missing transverse momentum. For the remaining *3L on-Z* signal region, we consider instead the transverse mass of the system made of the missing momentum and the lepton that is not part of any OSSF pair,

$$M_T = \sqrt{2p_T^{miss}p_T^l\left(1-\cos(\Delta\phi(\vec{p}_l,\vec{p}_T^{miss}))\right)}. \tag{5.3}$$

The comparison of the CMS distributions with those obtained with our MadAnalysis 5 reinterpretation is presented in Figure 5.1 and Figure 5.2. For interpreting properly the results of the shape comparison, we make use of two indicators.

- We first rely on the relative difference, on a bin-by-bin basis, between the number of events selected by the CMS analysis ($N_{\rm CMS}$) and the one selected in the recast analysis ($N_{\rm MA5}$). This difference is normalized with respect to the CMS predictions,
$$\delta(\text{bin}) = \frac{N_{\rm MA5}(\text{bin}) - N_{\rm CMS}(\text{bin})}{N_{\rm CMS}(\text{bin})}. \tag{5.4}$$
Such an indicator allows us to quantify the deviations between the CMS results and the recast predictions. We must however keep in mind that a large value in this indicator may not only be explained by the difference in the fast detector simulation or in the analysis implementation in MadAnalysis 5, but also by the statistical uncertainties inherent both to the samples used by CMS for the extraction of the official results (which we have no information on), and the validation samples.
- As mentionned in the previous item, the CMS official paper does not include information on the statistical uncertainties on the signal events. It is therefore impossible to assess the precision of their predictions. For the recast analysis, the bin-to-bin statistical uncertainties related to the amount of generated signal events at the end of the selection can be evaluated according to a Poisson distribution with variance
$$\sigma(\text{bin}) = \frac{N(\text{bin})}{\sqrt{N_{MC}(\text{bin})}}, \tag{5.5}$$
where $N_{MC}(\text{bin})$ is the number of surviving unweighted events in a specific bin at the end of the selection. We choose to define a relative indicator δ_{MC} quantifying the statistical uncertainties as
$$\delta_{MC}(\text{bin}) = \frac{1}{\sqrt{N_{MC}(\text{bin})}}. \tag{5.6}$$

In the results shown in Figure 5.1 and Figure 5.2, we can see that the shapes of the distribution are generally quite well reproduced. For all signal regions but the *4L OSSF1* one, the relative difference is less than 20–30%. Such an order of magnitude is consistent with the theoretical and statistical uncertainties related to the signal, and the built-in differences in the analysis code and the detector simulation. For the signal region *4L OSSF1*, a larger difference is observed for the first bin, but it also corresponds to a configuration in which the recast analysis lacks statistics. The indicator δ_{MC} indeed exhibits a high statistical uncertainty. The differences between CMS and MadAnalysis 5 are therefore considered as non-significant, an agreement being found in all the other bins, and we consider the implementation of the type-III seesaw signal regions as validated.

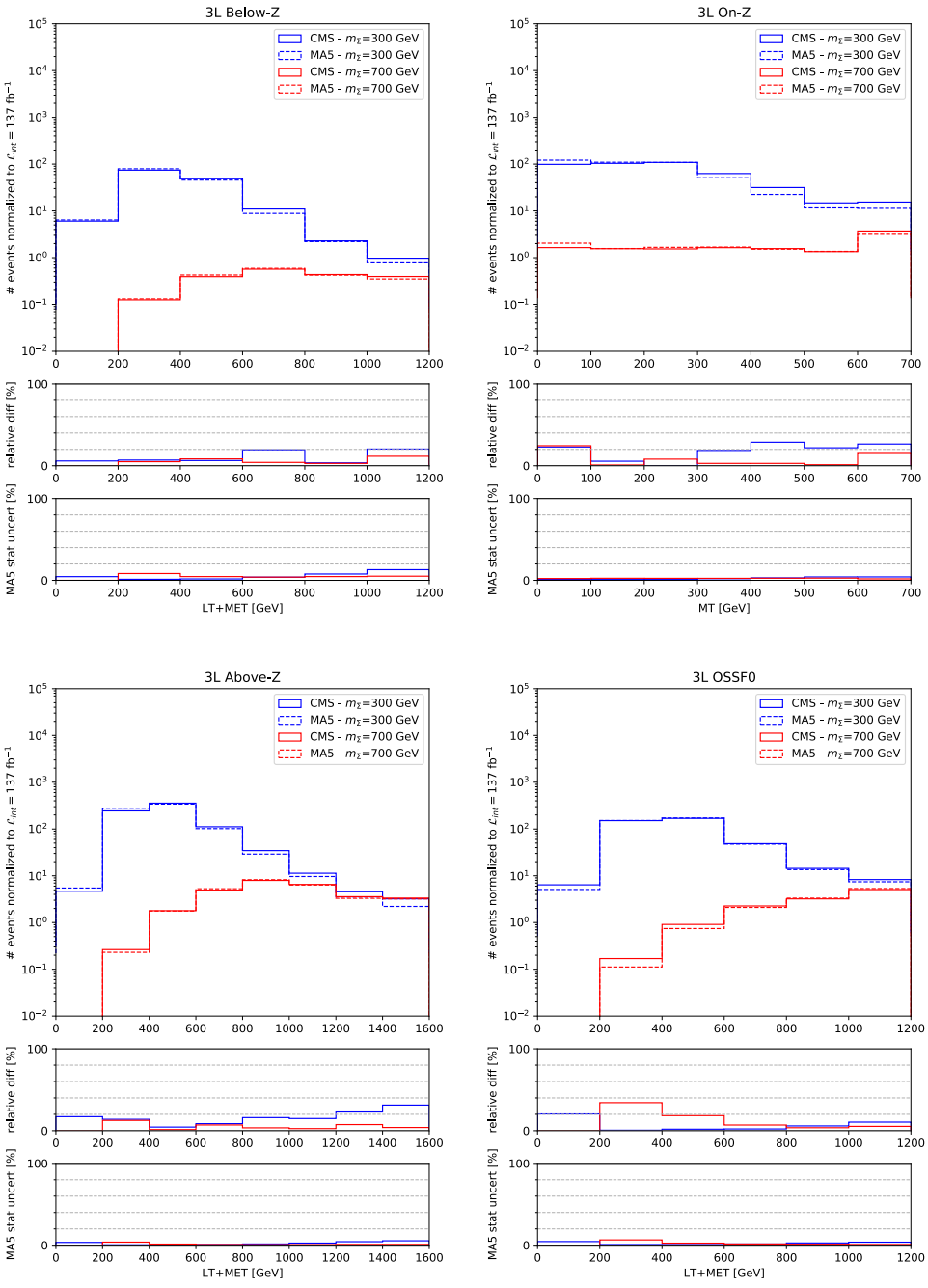

Fig. 5.1. Comparison between CMS official distributions and the corresponding MadAnalysis 5 predictions. In the main panel, we present distributions for the trilepton signal regions dedicated to probing type-III seesaw models. The last bins contain the overflow. In the central insets, we show the bin-to-bin relative difference δ(bin) in percent between the CMS and MadAnalysis 5 values, and in the lower insets, we indicate the statistical uncertainty δ_{MC}(bin) in percent related to the Monte Carlo samples used for the MadAnalysis 5 predictions. The distributions in red and blue correspond respectively to scenarios with a Σ mass set to 700 GeV and 300 GeV.

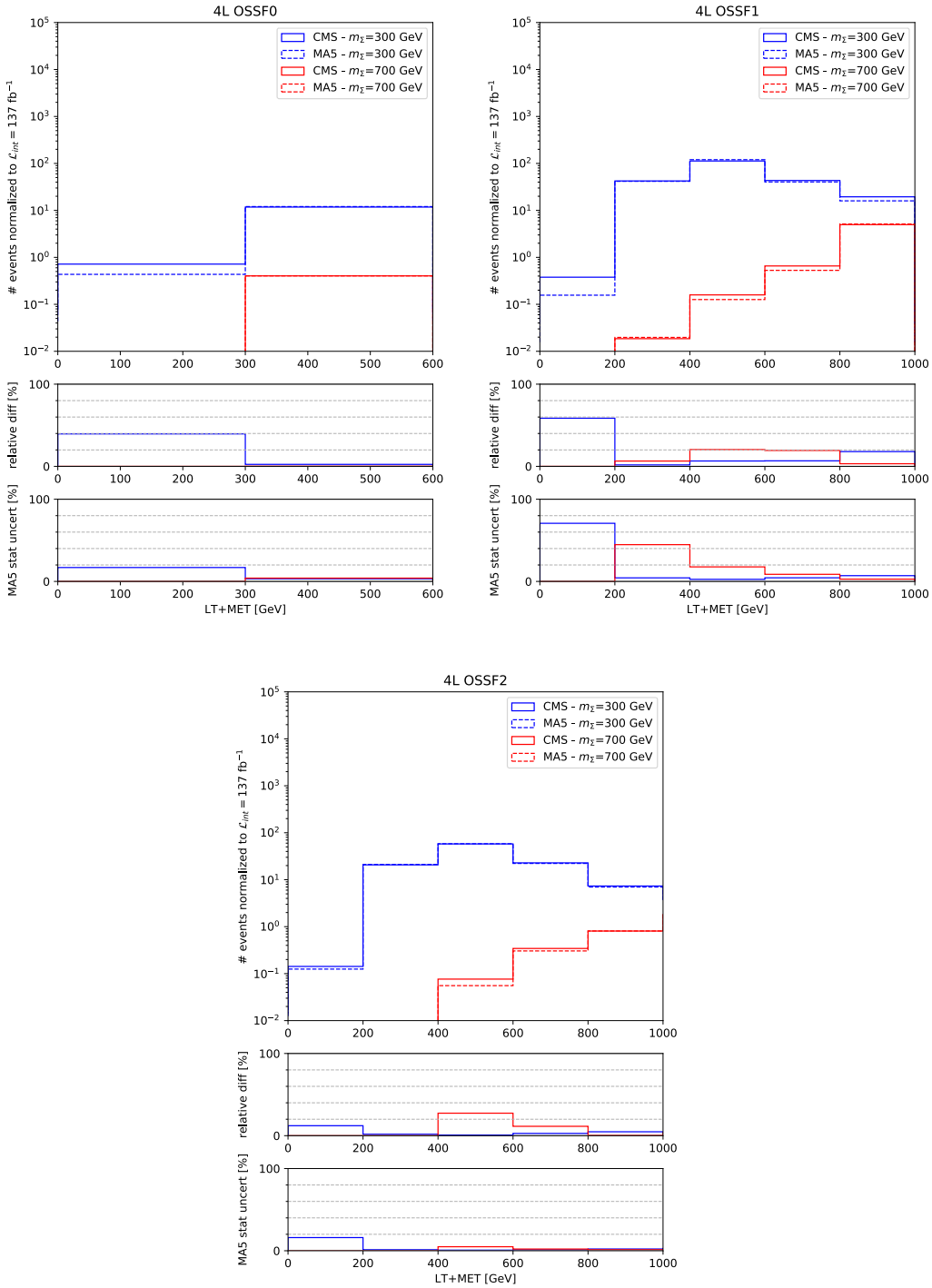

Fig. 5.2. Same as in Figure 5.1 but for the four-lepton seesaw signal regions.

ϕ scalar/pseudoscalar	ϕ mass	ϕ decay	Number of produced events
pseudoscalar	20 GeV	$\phi \to \mu\mu$	2,400,000
		$\phi \to ee$	4,400,000
scalar	70 GeV	$\phi \to \mu\mu$	2,400,000
		$\phi \to ee$	3,200,000

Table 5.5: List of produced signal samples for the validation of the $t\bar{t}\phi$ signal regions.

5.4. *Validation of the implementation of the $t\bar{t}\phi$ signal regions*

5.4.1. *Event generation*

To validate our implementation of the $t\bar{t}\phi$ signal regions, we consider a simple model implemented in FeynRules. It includes a new light CP-even scalar or CP-odd pseudoscalar boson, labeled ϕ, which can is produced at the LHC through its Yukawa coupling g_t to top quarks. The corresponding UFO model [100, 104] has been connected to MG_aMC@NLO in order to produce events at LO in QCD.

We produce the new boson ϕ in association with a top-antitop pair via its coupling g_t, and we assume that ϕ decays into a pair of charged leptons (electrons or muons) via a Yukawa coupling labeled g_l. The cross sections are calculated with the NNPDF3.0 LO set of PDF in the case where the product $g_t \cdot BR(\phi \to l^+l^-)$ is equal to 0.05, and read 0.02160 ± 0.00216 pb for a pseudoscalar boson with a mass of 20 GeV, and to 0.06597 ± 0.00660 pb for a scalar boson with a mass of 70 GeV [101]. The associated theory errors are taken as reported by the CMS collaboration as no information is provided on how they have been evaluated. Concerning the (anti-)top quark, the decay into Wb is forced with a branching ratio of 1, and the W decay is handled by Pythia 8. Trilepton and four-lepton final state can arise from leptonic W-boson decays.

Pythia 8 is used in order to handle parton showering, hadronization, and the simulation of the underlying events (multiple interactions and beam remnant interactions). The underlying events tune is chosen to be CP5 [105].

A large statistics of events have been generated for each ϕ mass value and for each decay channel, as listed in Table 5.5.

5.4.2. *Comparison with CMS results*

Public results provided by the CMS collaboration only consist of spectra of observables at the end of the selection. We therefore validate our implementation by comparing the distributions obtained with MadAnalysis 5 with the ones presented by CMS in Figures 5–10 of the analysis note. For low-mass ϕ (it is the case of our validation sample), the represented quantity is chosen to be the single attractor mass M^{20}_{OSSF}. The latter is defined as the invariant mass of the opposite-sign same-flavor lepton pair (OSSF) that is the closest to 20 GeV. Comparisons are performed in Figures 5.3, 5.4, 5.5, 5.6 and 5.7 for all $t\bar{t}\phi$ signal regions.

At first order, the recast analysis manages to reproduce quite well the distributions presented in the CMS paper. There are however noticeable differences. The two indicators δ(bin) and δ_{MC}(bin) defined in Section 5.3.2 are once again used for the interpretation of our findings and to quantify the level of agreement.

The statistics used for the validation of the recast analysis seems to be enough because the δ_{MC}(bin) indicator is less than 10% for all signal regions. For signal regions in which the relative difference between the CMS and the recast predictions is large, we find first that the issue holds independently of the ϕ decay channel. The findings however allow us to interpret this difference as a consequence of a lack of statistics in the events used by the CMS collaboration (on which information is not provided). We can indeed observe that the CMS predictions are plagued with important statistical fluctuations, that are much larger than in the recast analysis. We therefore consider our implementation validated, at least at a level representative of what could be done with the information made public by the CMS collaboration.

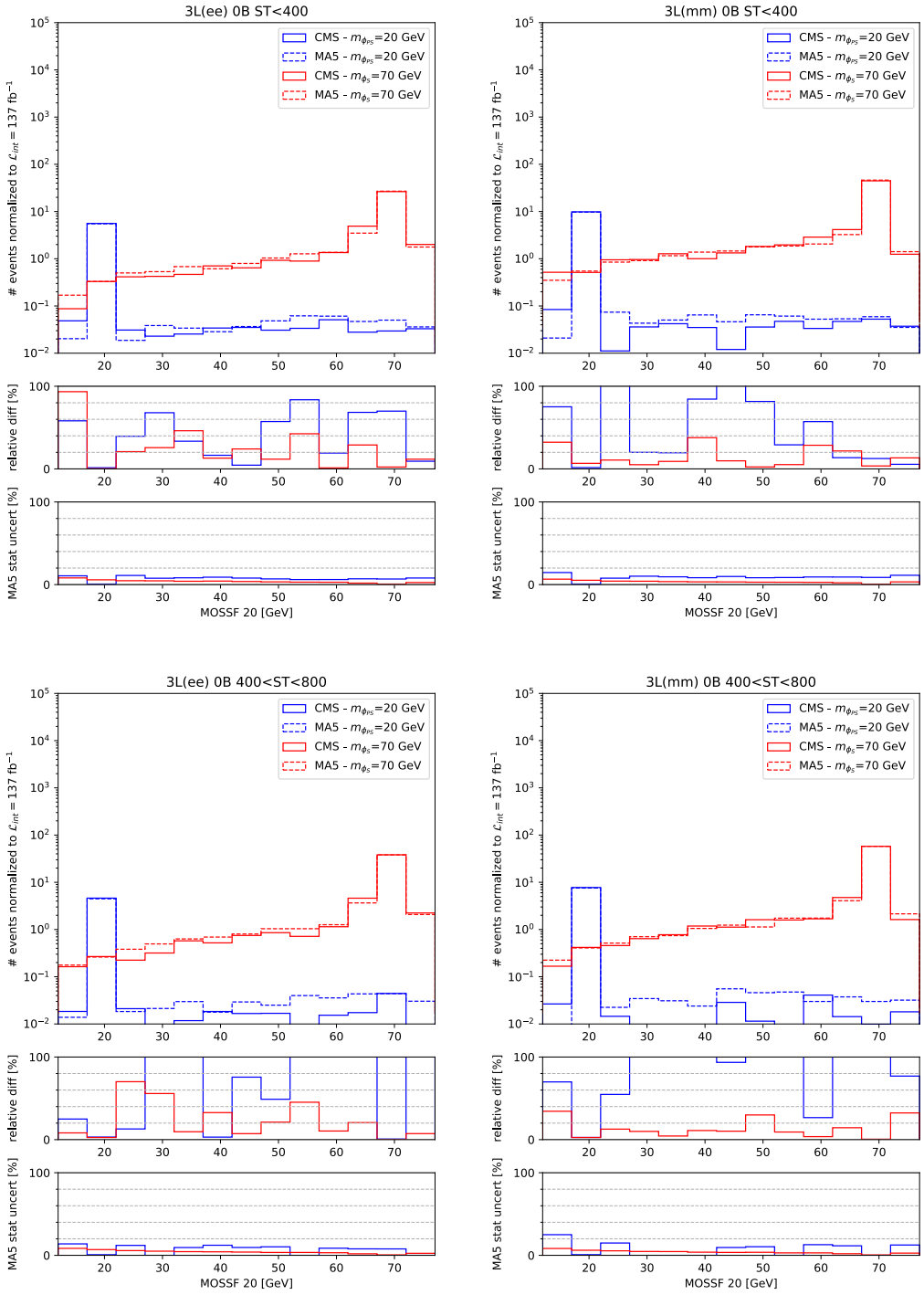

Fig. 5.3. Same as in Figure 5.1 but for the first four trilepton signal regions dedicated to probing the $t\bar{t}\phi$ model. The distributions in red and blue correspond respectively to scenarios with a scalar of mass of 70 GeV, and a pseudoscalar of mass of 20 GeV.

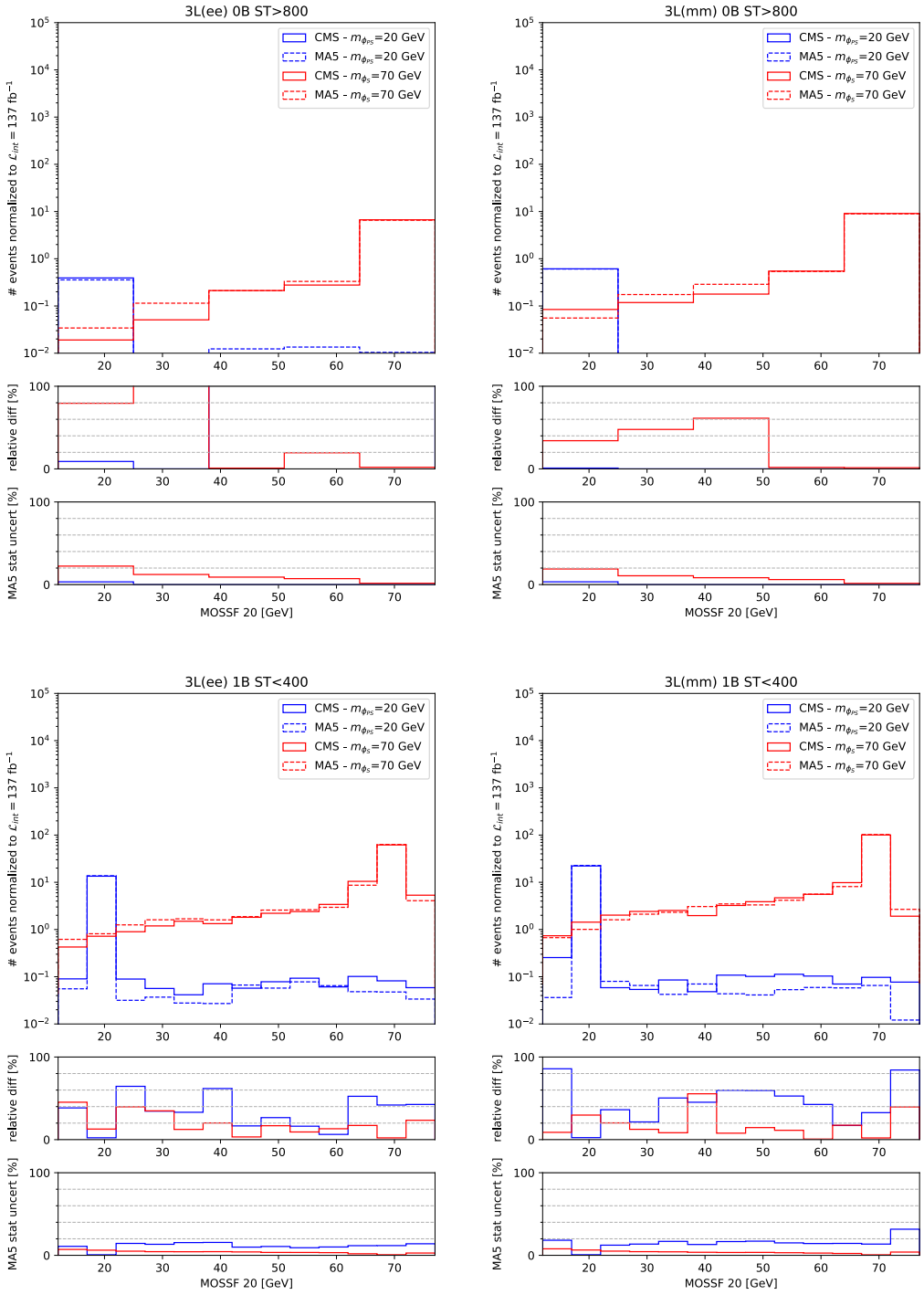

Fig. 5.4. Same as in Figure 5.1 but for the next four trilepton signal regions dedicated to probing the $t\bar{t}\phi$ model. The distributions in red and blue correspond respectively to scenarios with a scalar of mass of 70 GeV, and a pseudoscalar of mass of 20 GeV.

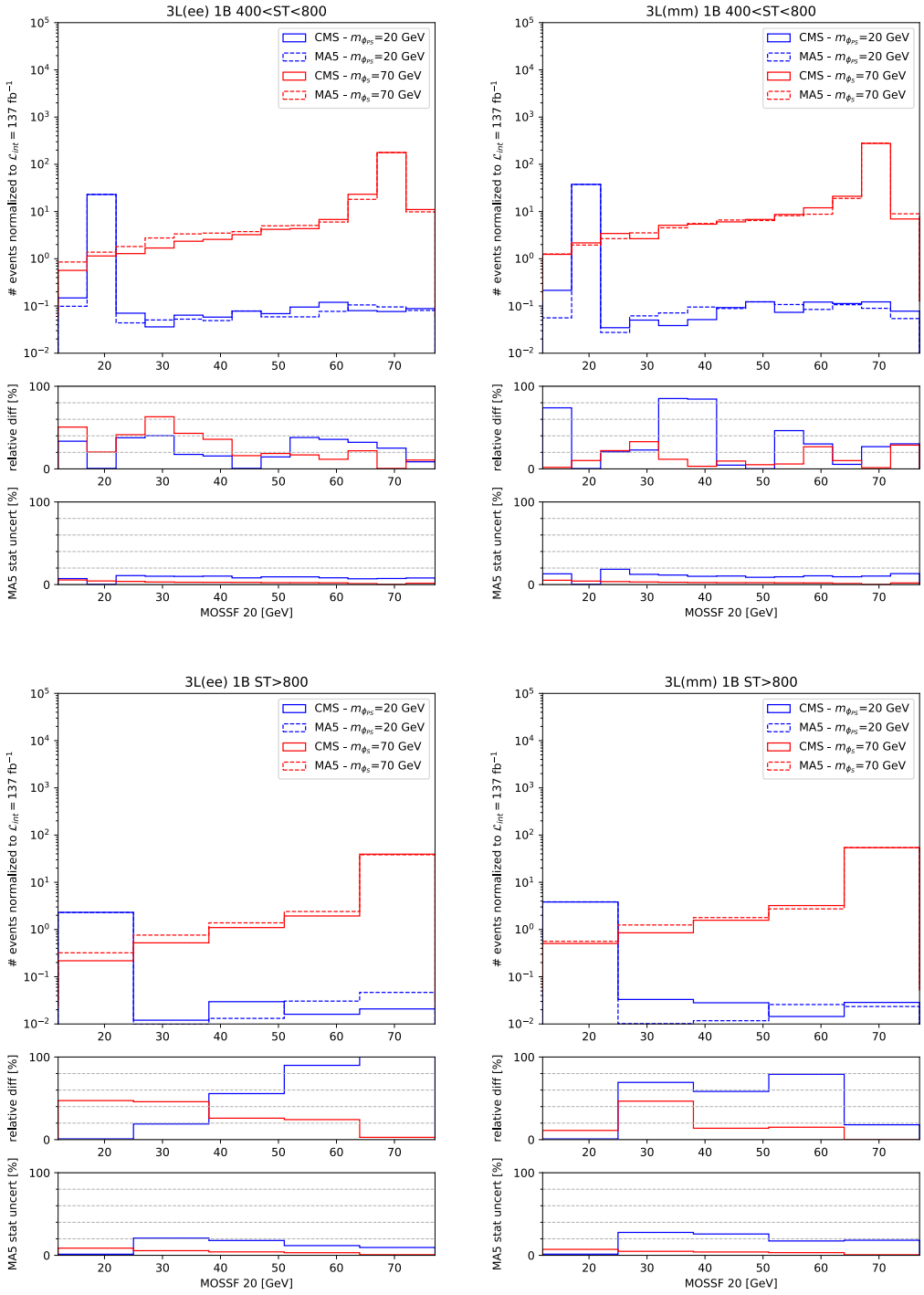

Fig. 5.5. Same as in Figure 5.1 but for the last four trilepton signal regions dedicated to probing the $t\bar{t}\phi$ model. The distributions in red and blue correspond respectively to scenarios with a scalar of mass of 70 GeV, and a pseudoscalar of mass of 20 GeV.

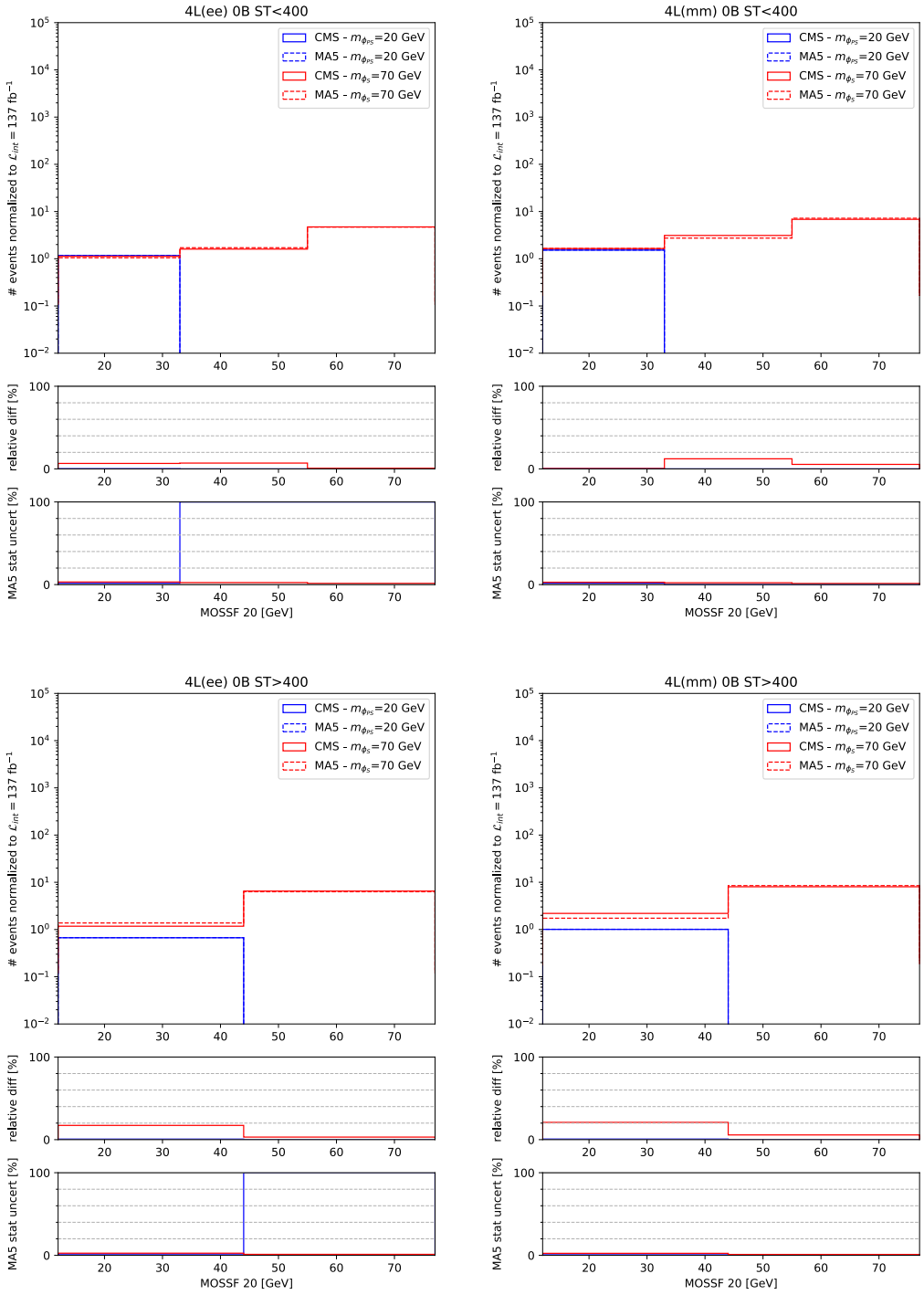

Fig. 5.6. Same as in Figure 5.1 but for the first four four-lepton and no b-jet signal regions dedicated to probing the $t\bar{t}\phi$ model. The distributions in red and blue correspond respectively to scenarios with a scalar of mass of 70 GeV, and a pseudoscalar of mass of 20 GeV.

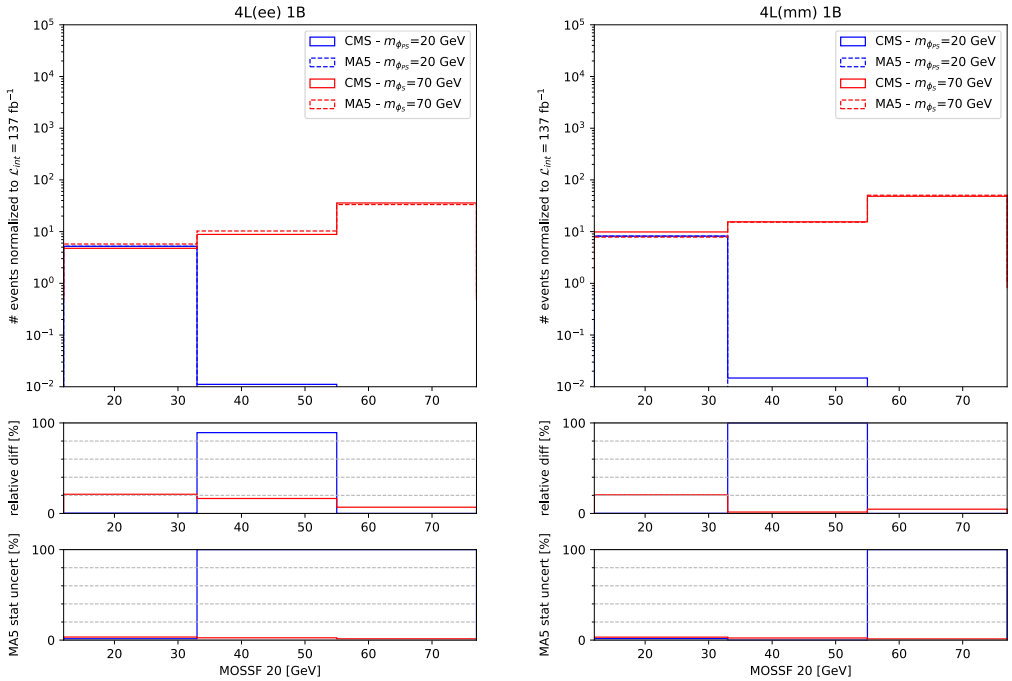

Fig. 5.7. Same as in Figure 5.1 but for the last two four-lepton and no b-jet signal regions dedicated to probing the $t\bar{t}\phi$ model. The distributions in red and blue correspond respectively to scenarios with a scalar of mass of 70 GeV, and a pseudoscalar of mass of 20 GeV.

5.5. *Conclusions*

We have presented the implementation of the multileptons search CMS-EXO-19-002 in the MadAnalysis 5 framework. This search considers proton-proton collisions at $\sqrt{s}$ = 13 TeV and an integrated luminosity of 137 fb^{-1}. Samples of signal events relevant for both the type-III seesaw and $t\bar{t}\phi$ signal regions have been generated with MadGraph5_aMC@NLO at LO, then proccessed by Pythia 8 for parton showering, hadronization and mutiple parton interactions, and by Delphes 3 for the detector simulation. We have compared predictions made by MadAnalysis 5 with the official results provided by the CMS collaboration. The only public material for validation consist in key-observable distributions at the end of selection. We have considered various benchmark scenarios in both the electron and muon channel. The shapes of the distributions have been compared and are correctly reproduced for the seesaw signal regions. Discrepancies are found in the case of the $t\bar{t}\phi$ events, in particular in the trilepton channels. These can however be explained mainly by a lack of statistics of the CMS paper.

The MadAnalysis 5 C++ code is available, together with the material used for the validation of this implementation, from the MA5 dataverse (https://doi.org/10.14428/DVN/DTYUUE) [21].

Acknowledgments

We are very grateful to Yeonsu Ryou Juhee and Song and Kihong Park who have in the first place begun to work on this implementation. We are also indebted to Benjamin Fuks for his help and patience. We sincerely thank the organizers of the second MadAnalysis 5 workshop for their warm welcome in Seoul and the success of the event.